Numerical modeling of ocean swell contributions to the global wind-wave climate ☆

Jose-Henrique G.M. Alves [*],[1]

SAIC/GSO at Marine Modeling and Analysis Branch, EMC/NCEP/NOAA 5200 Auth Road, Room 209, Camp Springs, MD 20746, United States

Abstract

A new technique for studying the contribution of ocean swell to the global wind-wave climate is proposed, on the basis of numerical simulations of wind-wave evolution. In this technique, waves are generated by winds that are kept active only in selected oceanic areas and switched off over the rest of the global ocean domain. In this way, swells are generated only in selected areas and are propagated freely elsewhere. A preliminary analysis of the major patterns associated with swells generated within a selection of generation areas is presented, providing new insights on the properties of swell propagation. Results support the validity of the technique for the purposes of wind-wave climate studies on a global scale.
© 2005 Elsevier Ltd. All rights reserved.

1. Introduction

Wind-waves generated by intense storms become ocean swells as they leave their generation zone, traveling long distances across the globe. Empirical data supports the idea that windseas and swells together account for more than half of the energy carried by all waves on the ocean surface, surpassing

---

the contribution of tides, tsunamis, coastal surges, etc. (Kinsman, 1965). Investigations on the contribution of ocean swell to the wind wave climate are, therefore, of great importance in a wide range of oceanographic studies, coastal management activities and ocean engineering applications.

Seminal papers by Munk (1947); Barber and Ursell (1948); Munk et al. (1963) and Snodgrass et al. (1966) [henceforth referred collectively as EWOS, for early works on swell] provided important insights on swell generation and propagation that have stood the proof of time, and are still valid paradigms today. Studies conducted over the last three decades have expanded these initial insights, revealing that the presence of swell affects several important processes at the air–sea interface, such as the modulation, blockage and suppression of short wind-generated waves (Donelan, 1987; Shyu and Phillips, 1990; Chen and Belcher, 2000), the modulation of the surface stress vector and changes to the structure of the atmospheric boundary layer (Donelan et al., 1997; Drennan et al., 1999; Grachev and Fairall, 2001; Grachev et al., 2003; Smedman et al., 2003), for example. These new and challenging issues have renewed the interest of the scientific community, motivating the publication of several recent papers on the topic of swell propagation (e.g., Hanson and Phillips, 2001; Chen et al., 2002; Ardhuin et al., 2003a,b).

In this study, a technique is introduced that allows an evaluation of the contribution of swells from different ocean basins to the global wind-wave climate. The conceptual basis of such a technique is built upon the EWOS, leading to an experimental framework based on the following assumptions. First, swell systems are generated in quasi-discrete oceanic areas with a high incidence of intense and persistent storms. Second, waves generated within these areas propagate freely throughout the global ocean, not significantly changing due to interactions with local winds and waves outside the generation area. Finally, it is assumed that the importance of local effects such as shoaling, diffraction and wave-current interactions are secondary and may be neglected.

The selection of originating or swell-generation areas is based on an analysis of a combined historical storm database. Numerical simulations of wind-wave evolution within these areas are carried out using the surface wind fields from NCEP's global numerical weather prediction model. Experiments are made in which wind fields are kept active in each individual selected area, while being switched off in the rest of the global ocean domain. This allows waves generated in selected areas to propagate freely as swell to other regions of the globe. Results presented below consider a 2-year simulation period and swell systems from 13 originating areas.

The remainder of this manuscript is organized as follows. Section 2 describes the general methodology for simulating swell generation and propagation. The general basis for selecting swell-generation areas is described in Section 3. The numerical modeling approach and experimental strategy are outlined in Section 4. A brief discussion in Section 5 focuses on an examination of how realistically the segmented swell fields represent the full, unsegmented wave fields. Section 6 presents a brief analysis of the major swell propagation patterns, highlighting the potential of the technique for broader swell climatology studies. Finally, concluding remarks and suggestions for future research are made in Section 7.

2. General methodology

Spectral partitioning is the approach commonly used to isolate the contributions of windseas and swell at a given location. This technique, introduced by Gerling (1992), consists of dividing

the wave spectrum into subsets representative of individual wave fields. It generally uses ad hoc criteria based on spectral shape, properties of the local wind field and assumed parametric spectral formulations, among others. A review of existing techniques and new insights on spectral partitioning are provided by Hanson and Phillips (2001).

The present investigation uses an alternative approach for separating the contribution of multiple swell fields at a given point. Based on the findings reported in the EWOS papers, the following assumptions are made about swell propagation on a global scale:

- Away from the generation zone, swell properties are not significantly affected by surface winds.
- Swells undergo negligible energy loss due to viscous dissipation or whitecapping.
- Swells are not significantly modified via interaction with co-existing wave systems.
- Swell propagation is well approximated by linear wave theory.
- Deep water swell propagation follows great circle paths exclusively.
- In shallow and intermediate waters, swells are modified through refraction only.
- Swell energy is totally dissipated at land boundaries.
- Local effects (shoaling, diffraction and wave-current interactions) are negligible.

In view of recent observations and theoretical reasoning, the first three assumptions above are the most controversial. EWOS data support their validity for swells with periods higher than 15 s, indicating also that waves with periods between 10 s and 15 s may or may not suffer noticeable decay. The ambiguous behavior observed in the latter case is likely a result of effects that went undetected by the now obsolete technology used in the measurements reported by the EWOS.

Recent studies indicate that swell decay rates may be affected by a reverse momentum flux mechanism triggered whenever swells travel faster than surface winds (Donelan et al., 1997; Drennan et al., 1999; Grachev and Fairall, 2001; Smedman et al., 2003). On the other hand, new theoretical arguments have hinted that although wave-turbulence interactions may contribute to swell decay, they could also cause energy transfers from windseas to swells (Teixeira and Belcher, 2002; F. Ardhuin, personal communication, 2004). The degree to which these processes cancel each other or add up is still unknown. Therefore, their effects to the results below may only be assessed in the future, when new data become available.

The assumption that the effect of currents is negligible may also seem unjustified in strong oceanic jets found near the Drake Passage and in the Gulf Stream, where current speeds peak at 0.5 m/s (Klinck and Nowlin, 2001) and 2.0 m/s (Gill, 1982), respectively. However, even in such strong currents changes in simulated swells are not expected to be very significant on a larger scale. For instance, transformations of swell height and direction caused by the Gulf Stream jet computed by Holthuijsen and Tolman (1997) were of the order of less than 10% and 10°, respectively. For the present study, these are not expected to be significant considering typical observation errors and other uncertainties on the numerical modeling side due to wind and wave model resolutions, for example.

Under the working hypothesis of this study, relevant swell systems evolve from wave fields generated locally (windseas) by strong winds associated with intense extratropical (mid-latitude) and tropical storms (including hurricanes, typhoons, etc.). Windseas generated in these intense storms

gradually evolve into ocean swell as wave components with different length scales disperse, propagating away from the generation zone.

In this idealized framework, if the generation of windseas by a number of independent storms co-existing at any given time is simulated in isolation, the resulting swell fields may be investigated individually as they propagate away from the originating storm. In each of these model simulations, storms would be isolated by switching off wind fields outside the storm's area of influence. Wave fields generated by an isolated storm would then be allowed to propagate freely away from the generating area and throughout the global ocean as swell.

Assuming that the principle of superposition of linear wave components, and that all other assumptions made above are valid in such a context, the above wind field segmentation approach would allow for the reconstruction of the total wave field at any given point from the cumulative contributions of each individual "segmented" wave/swell system. These segmented swells would have been, by definition, partitioned from the beginning so their sources and individual properties would be fully determined in a straightforward manner.

Several limitations and difficulties obviously arise in this storm-by-storm wind field segmentation approach. The most challenging tasks include: (i) choosing criteria for fully isolating storms; (ii) determining the extent of storm durations and swell residence time and (iii) consistently merging and splitting complex events, etc. Another limitation of a storm-by-storm approach arises from computational costs involved in simulating a large number of individual storms throughout a period long enough to produce a global climatology.

From a physics perspective, the two most challenging assumptions are that: (i) swell-generating storm systems can be fully isolated; and (ii) while windseas transition to swells, there is no interaction with other co-existing winds or wave fields. While the latter is an acceptable assumption for swells that have traveled far enough from their originating storms, it is unlikely to hold for transitional areas just outside storm limits. Most of the problems of the idealized storm-by-storm approach are minimized by simplifying the wind field segmentation approach as follows.

Rather than isolating individual storm systems, a small number of discrete areas with a high occurrence rate of intense storms is selected. The validity of this simplified wind segmentation approach requires that the selected areas satisfy some basic constraints. First, these zones should contain the majority of storms belonging to a given region. Second, they should encompass the majority of tracks these storms follow over the ocean surface. Finally, generation zones should be separated by transitional "corridors" where the storm densities are typically low. Details on how swell generation zones that approximately satisfy these criteria were selected for the present investigation are discussed in the next section.

3. Swell generation areas

Previously-reported storm climatologies (e.g., Simmonds and Keay, 2000; Keable et al., 2002; Gulev et al., 2001; Lambert et al., 2002; Paciorek et al., 2002; Sinclair, 2002) show that it is, in principle, possible to define discrete oceanic areas encompassing intense storms with similar properties, along with most of their tracks. In this context, a fairly objective method to define storm generation areas has been developed using historical storm data combined from the atlas
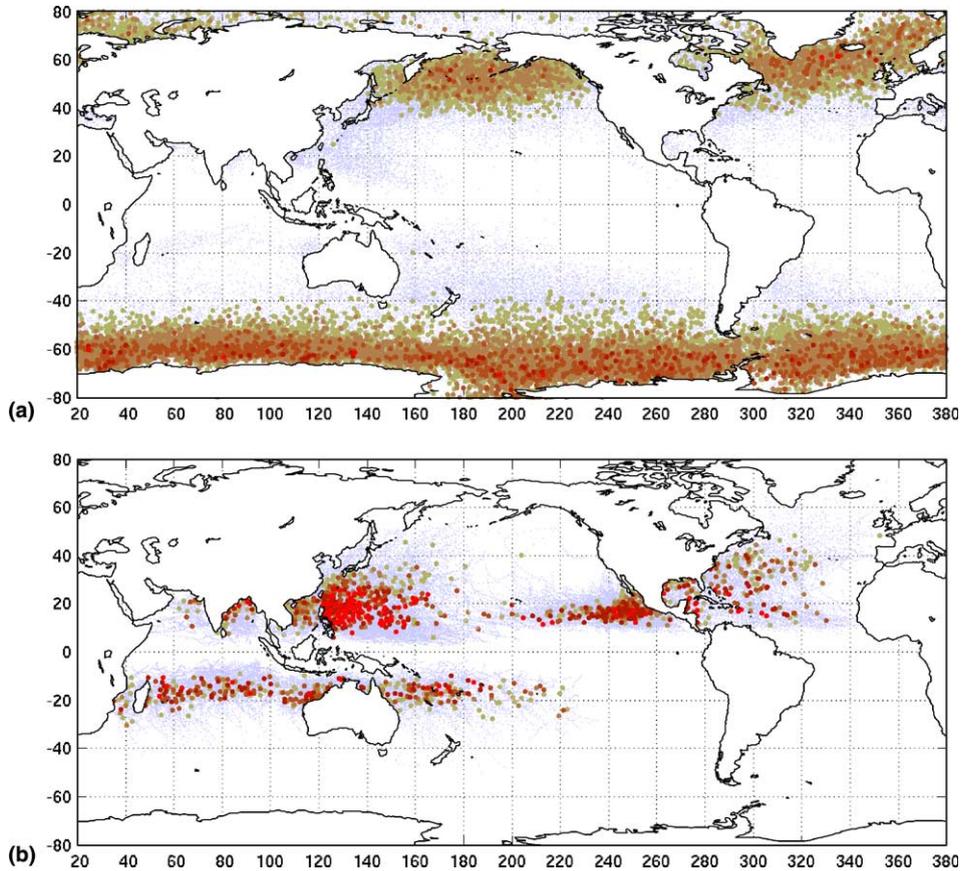
Fig. 1. Storm tracks (light dots) and points of maximum intensity (dark circles). Storm tracks from the GISS/NASA extratropical storm atlas are shown in (a). (b) Shows a combination of hurricane track data from NHC/NOAA and JTWC/US Navy.

of extratropical storm tracks of the Goddard Institute for Space Studies, GISS/NASA,[2] the hurricane best track files HURDAT of the National Hurricane Center, NHC/NOAA,[3] and the tropical cyclone best track data of the Joint Typhoon Warning Center, JTWC/USA Navy.[4] Data from these sources were reduced to a common period of 30 years (1971–2000), resulting in the combined storm database illustrated in Fig. 1.

Three parameters have been used for selecting swell generation areas:

- The number of points representing storm maxima.
- The number of discrete storm track locations.
- The number of tracks not crossing area boundaries (non-interrupted tracks).

---

[2] http://www.giss.nasa.gov/data/stormtracks/.
[3] http://www.nhc.noaa.gov/pastall.shtml.
[4] http://www.npmoc.navy.mil/jtwc/best_tracks/.

These parameters are calculated for individual storm histories in the combined storm database.

A set of first-guess generation areas was defined based on qualitative information gathered from a preliminary literature review. These initial areas were then redimensioned iteratively using data from the combined historical storm database, as follows. Storm tracks within a chosen area were extracted, providing the total number of observed storms, their maximum intensity points and a complete ensemble of discrete track location points per storm. Based on this information, the total numbers of storm maxima and track location points found within a discrete area were determined. Non-interrupted tracks were defined as tracks that had at least 3/4 of their location points within the selected area. Areas were redesigned to maximize the number of non-interrupted tracks.

Many storms in the combined database were either too short-lived or had intensities that were too low compared to the wind fields typically associated with the generation of swell systems reported in the literature (EWOS papers; Hanson and Phillips, 2001). Therefore, a subset retaining only intense storm systems was selected from the complete database using the following additional ad hoc constraints: (i) storms that had at least two track points; and (ii) storms that had at least one track point with surface pressure of 1000 mb or less (extratropical storms) or with maximum surface winds reaching category one or higher in the Saffir–Simpson scale (tropical storms).

Final areas were established as a compromise between maximizing the number of non-interrupted tracks and minimizing the computational effort, since the number of selected areas would determine the number of numerical experiments to be performed. Fig. 2 shows the 13 selected swell generation areas, which were mutually exclusive and covered the main oceanic areas of
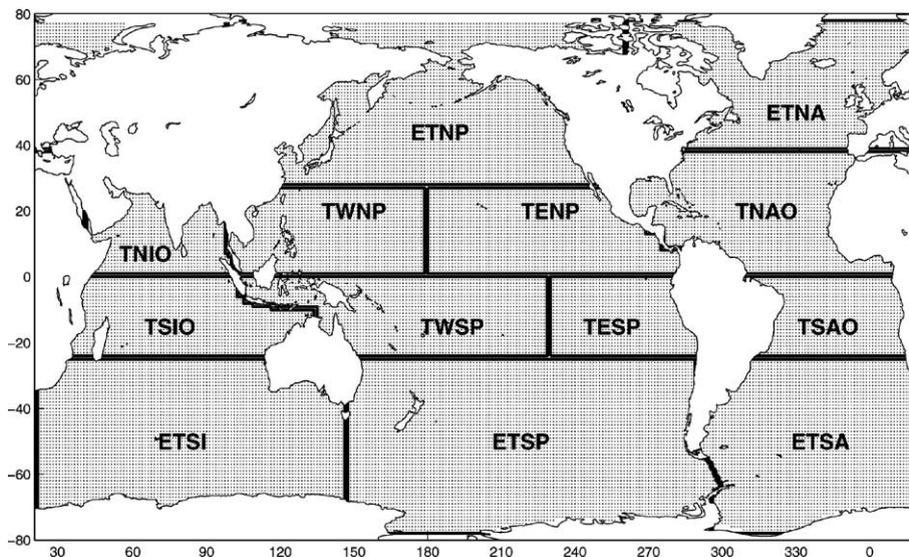
Fig. 2. Selected swell generation areas: tropical north Indian (TNIO), tropical western North Pacific (TWNP), tropical eastern North Pacific (TENP), tropical North Atlantic (TNAO), tropical south Indian (TSIO), tropical western south Pacific (TWSP), tropical eastern south Pacific (TESP), tropical south Atlantic (TSAO), extratropical North Pacific (ETNP), extratropical North Atlantic (ETNA), extratropical south Indian (ETSI), extratropical south Pacific (ETSP) and extratropical south Atlantic (ETSA).

Table 1
Yearly number of storms (N_{ST}), average storm life in days (T_{SL}) and percentage scores for numbers of storm maxima (N_{SMAX}), track point locations (N_{TPOS}) and non-interrupted tracks (N_{NIT}) at selected areas

Area	Extratropical storms					Tropical storms				
	N_{ST} (p/yr)	T_{SL} (days)	N_{SMAX} (%)	N_{TPOS} (%)	N_{NIT} (%)	N_{ST} (p/yr)	T_{SL} (days)	N_{SMAX} (%)	N_{TPOS} (%)	N_{NIT} (%)
ETSA	146	3.6	9.9	10.4	78.3	<1	–	–	–	–
ETSP	231	3.6	20.3	19.6	86.9	2	6.5	<1	<1	25.0
ETSI	207	3.6	16.4	15.6	82.5	3	6.9	<1	<1	28.6
ETNA	277	3.7	24.9	24.0	85.1	15	6.3	1.2	2.0	23.5
ETNP	276	3.7	23.1	23.3	88.8	10	8.3	3.6	6.3	10.9
TSAO	3	2.5	<1	<1	73.3	<1	–	–	–	–
TESP	<1	–	–	–	–	<1	–	–	–	–
TWSP	11	4.5	<1	<1	76.5	5	8.9	10.0	8.4	86.0
TSIO	6	4.0	<1	<1	80.2	7	9.8	14.7	14.2	92.8
TNAO	36	3.8	<1	1.6	64.8	5	10.6	11.5	10.4	80.5
TENP	4	4.4	<1	1.8	80.0	10	8.6	20.7	18.6	96.6
TWNP	17	5.0	<1	1.7	85.3	17	10.6	34.0	34.7	81.6
TNIO	17	2.4	1.8	1.2	98.6	2	7.2	3.6	2.7	91.5

the globe. Relative scores obtained for the selected areas in terms of the criteria defined above are shown in Table 1. This table also indicates the number of tropical and extratropical storms per year and their average duration in each selected area.

Data in Table 1 indicate that more than 90% of all extratropical storm maxima N_{SMAX} around the globe are contained within selected discrete extratropical areas. Similarly, the tropical storm areas contain more than 95% of tropical storm maxima in the chosen storm database. Table 1 further reveals that two selected areas, TSAO and TESP, are nearly free of storms of any kind.

Other properties of intense storms may be derived from a combined inspection of Fig. 1 and Table 1. For instance, extratropical areas in the Southern Hemisphere are almost completely free from penetration by tropical systems from adjacent tropical areas. Consequently, swell systems originating from these areas will have been generated almost exclusively by extratropical systems. Furthermore, Table 1 reveals that the vast majority of storm systems contained in extratropical areas of the Southern Hemisphere (around 80% or more) reach their maximum intensity and have most of their track points contained within the selected area boundaries, despite the absence of actual physical boundaries.

Unlike in the Southern Hemisphere, Table 1 indicates that extratropical areas in the Northern Hemisphere, ETNP and ETNA, contain between 10 and 15 tropical storms per year. However, Fig. 1(b) reveals that most tropical storms entering ETNP and ETNA are likely the weaker, final stages of storms from neighboring tropical areas. This impression is also supported by the low percentage of non-interrupted tropical storm tracks within ETNA and ETNP seen in Table 1. Considering further that tropical systems correspond to less than 10% of the yearly storm count in these areas, it is assumed that swell systems originating from ETNA and ETNP are predominantly, but not exclusively, generated by extratropical systems.

In most cases, tropical areas enclose a significant number of systems included in the extratropical storm count of the GISS/NASA atlas, as seen in Table 1. Within TSIO and TENP, a

substantial number of these "extratropical" systems occur during the *summer*. Since the automatic storm tracking approach used by GISS/NASA does not filter out tropical systems (Mark Chandler, GISS/NASA, personal communication 2004), it is likely that the storms counted within TSIO and TENP as extratropical are actually tropical systems. This "double count" hypothesis, supported by track data illustrated in Fig. 1 for TSIO and TENP, does not seem to hold for other tropical areas.

Fig. 1 indicates that although the number of extratropical storm maxima occurring in tropical areas is close to nil, TWSP, TNAO, TWNP and TNIO enclose a relatively large number of extratropical storm track location points. These "intruding" extratropical systems may not be directly discarded as a source of swell systems originating from these tropical areas. Fortunately, tropical storms occur almost exclusively during summer, whereas extratropical storms are observed in tropical latitudes predominantly during winter. Therefore, a seasonal analysis is used to differentiate the properties of swell systems generated by either extratropical or tropical storms within TWSP, TNAO, TWNP and TNIO.

Results described in this section show that the 13 selected extratropical and tropical swell generation areas shown in Fig. 2 contain the vast majority of storm maxima and track locations observed within any given ocean basin. Table 1 reveals further that most storm tracks observed within selected areas are not interrupted by chosen area boundaries. Therefore, it is assumed that the selected areas are representative, within the context of a storm climatology, of a climatologically consistent, self-contained swell generation area at a level compatible with the objectives of the present study.

4. Experimental framework

The generation and propagation of wave systems were simulated with the wind-wave model WAVEWATCH III, version 2.22 (Tolman, 2002a). Simulations were performed using a global model grid with a resolution of $1.25° \times 1°$ in longitude and latitude, respectively (Tolman et al., 2002). Wave growth was computed using source terms to account for wind input, non-linear wave–wave interactions and whitecapping. Propagation included the effects of depth-induced refraction and island shadowing/blocking (Tolman, 2003).

Wind and air–sea temperature difference fields, both used in the formulation of wind input in WAVEWATCH III, were obtained from hindcast archives of NCEP's wave prediction system, consisting of analysis data from the global atmospheric forecasting system (GFS) at NCEP/ NOAA (Moorthi et al., 2001). Winds from the GFS are reduced from the model's lowest vertical level (995 mB or ≈ 35 m) to the standard 10-m height assuming neutral stability, as described in Tolman (1998a). Simulations also included daily ice concentrations from NCEP's automated passive microwave sea ice concentration analysis (Grumbine, 1996).

Experiments consisted of model runs in which the generation areas were isolated one at a time by switching off (setting to 0) wind fields in all but the selected generation area. These experiments produced a two-year-long history of wind-wave generation scenarios and associated swell propagation independently for each of the 13 selected areas using the segmented wind fields. One control run with the unsegmented/complete global surface wind fields was also performed for verification purposes. Therefore, a total of 14 independent simulations were performed.

Each model run provided results for a simulation period starting on 1 January 2000 up to 1 January 2002. Although this period is obviously too short for generating a comprehensive climatology study, it was considered enough for the purpose of verifying the proposed technique. Simulations also included a one-month spin-up period starting on 1 December 1999. The spin-up guaranteed that all swell systems with long residence time were included. The chosen period reflected the availability of nearly continuous buoy data at selected validation sites. Such observational data will be used in a future study to investigate the contribution of swell to local wave climatology, using the wind segmentation approach introduced in the present study.

Although a comprehensive climatology analysis is beyond the scope of the present study, results from numerical experiments are used to illustrate the potential of the approach in studies that focus on a global-scale swell climatology. They also allow a qualitative description of global swell propagation patterns based on yearly or seasonal mean and maximum significant wave heights and on a persistence parameter, defined here as the number of days per year or season in which the swell significant wave height was above a 0.25 m threshold.

5. Verification of the wind segmentation technique

A straightforward but effective way of verifying the consistency of the swell-field segmentation approach is to reconstruct the full wave fields from the segmented swell fields, and to compare these reconstructed quantities to the control model run. This reconstruction of "total" wave fields from segmented runs is made by superposing the total energy contribution from each segmented field. Verification is made in terms of the bias and root-mean-square errors of the reconstructed total wave energies to the total wave energy fields from the control run.

Fig. 3 shows the global distribution of two-year mean annual bias and RMS error of the superposed energy from segmented wave fields, in percentage points relative to the total wave energy of the control run. Fig. 3 reveals that the magnitude of both the reconstructed wave field bias and RMS error in the vast majority of oceanic areas is smaller than 10–15%, which is close to the expected observational error of wind-wave measurements. Therefore, we may assume that such relative errors are generally within acceptable limits for the purposes of climatological studies in most oceanic regions. As expected, however, these two quantities peak near the boundaries of segmented swell-generation areas, revealing some interesting characteristics of the wave fields thereof.

The highest values of mean annual bias ($\approx$20–25%) and RMS error ($\approx$30–35%) are found near the zonal and meridional boundaries of TENP/TWNP and TESP/TWSP. The superposition of segmented fields provides, on average, an overestimation of the reference total energy levels in these regions, which are dominated by either swells from high latitudes or waves generated locally by trade winds. However, high values of error statistics propagate with the predominant easterly trade wind flow component, slightly intensifying in the TESP/TWSP (TENP/TWNP) boundary during southern (northern) Hemisphere summer and vice-versa. Higher errors are, therefore, primarily a result of the artificial interruption of these trade wind fetches with boundaries along the equator caused by the chosen numerical approach.

Other areas of higher values for error statistics are found near the meridional boundaries between ETSA, ETSP and ETSI, and near the zonal boundaries between most swell generation
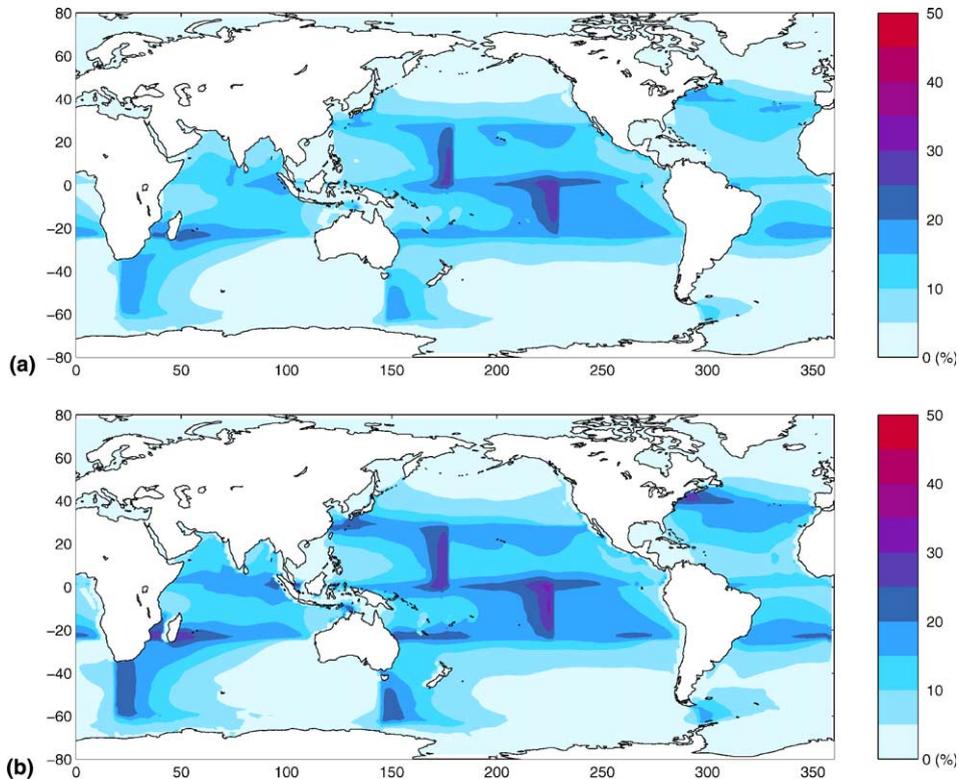
Fig. 3. Global distribution of error statistics for reconstructed wave fields relative to a reference run: (a) mean annual bias and (b) mean annual RMS error.

areas. Like in the case of interrupted trade wind flows, these larger errors are a result of the artificial interruption of dynamic fetches generated by the advection of intense storms or of static fetches developed in intense semi-stationary systems. Dynamic fetches develop when the energy carried by waves moves at the same speed and direction as the generating wind field advection. Regions of higher relative errors associated with the interruption of dynamic fetches appear generally as an eastward propagating signal in Fig. 3, near the boundaries of extratropical areas.

The cause of higher errors near area boundaries may be explained as follows. Artificial boundaries interrupt the coupling of waves and winds in long or moving fetches that would, in the control run, extend continuously over area boundaries. In the control run, continuous or dynamic fetches will generate wave fields with saturated high-frequency spectra throughout the extension of the fetch. These spectra will, therefore, no longer receive a positive net influx of energy in the high-frequency range.

On the other hand, reconstructing wave fields in fetches interrupted by area boundaries from multiple runs involves adding energy from two or more independent wave systems: the pre-existing waves propagating from an upwind area, with saturated high-frequency spectra, and the newly-generated windseas, with spectra that quickly saturate in the high-frequency range. These superposed spectra do not "see" each other because the simulations are made independently

for each selected area. Therefore, their superposition near area boundaries will lead to an overestimation of total energies.

Generally, higher relative errors are mostly limited to small regions near area boundaries, not propagating very far, as shown in Fig. 3. Therefore, they may be assumed to be of secondary importance for a large-scale global swell climatology study. Nevertheless, they provide some insight about potential sources of errors in local climatology studies. Furthermore, they highlight possible sources of errors in wave prediction systems with poorly-chosen spatial boundary conditions in the model grids of local/regional wind-wave models, whenever these local/regional grids are not nested onto larger-scale models.

In terms of a quantitative analysis, the interrupted growth of wave systems near area boundaries is a potentially serious limitation of the segmentation field approach. As argued above, this artificial effect breaks the continuous flow of energy from high- to low-frequency spectral components, due to non-linear wave–wave interactions. This is, in principle, expected to be a problem for swell evolution. Such a limitation, however, is attenuated in the context of a global climatology by the fact that, on average, less than 15% of intense storm tracks are interrupted within most generation areas (see Table 1).

Further validation would be possible by comparing reconstructed wave fields and spectra with measured data. The indirect evidence presented above, however, shows that reconstructed fields are consistent with the reference run, which is in all details a "carbon-copy" of the current operational wave forecasting system at NCEP/NOAA. This system has been extensively validated against buoy and altimeter measurements in both basin and global scales, as reported in Tolman (1998a,b); Wingeart et al. (2001); Tolman (2002b) and in NCEP's wave forecasting system web site.[5] Mean annual fields from model simulations made for the present study have also been compared qualitatively to data presented in Gulev and Hasse (1998) and Chen et al. (2002), showing good agreement. Therefore, it is reasonable to assume that reconstructed fields will be generally consistent with observations.

Based on the results presented so far, we may conclude that the segmentation of wind fields provides a valid framework for the purpose of studying climatological aspects of swell fields on a global scale. In the next section we apply this methodology to provide a preliminary analysis of global patterns of swell propagation, which highlights the potential of the proposed technique for more comprehensive global swell climatology studies.

6. Major swell propagation patterns

The analysis of results presented in this section will focus on a single representative wave field parameter, the significant wave height H_s. Global features of swell systems originating in the 13 selected generation areas will be explored through the analysis of the annual or seasonal averages of three statistical parameters derived from simulated H_s fields: mean, maximum and the previously defined persistence parameter.

---

[5] http://polar.ncep.noaa.gov/waves/validation.html.

When comparing results from the two simulation years presently considered, it was found that the qualitative properties of the global distributions of mean and maximum H_s and persistence were very similar. Therefore, our analysis of results will focus on simulations made using year 2000 data, although the analysis will be expanded to include information from year 2001 simulations whenever more significant differences were found. A description of the relevant seasonal differences in simulated patterns is also made whenever appropriate.

6.1. Extratropical storm areas

Table 1 indicates that the largest number of yearly storms in chosen areas occurs in extratropical areas of the Northern Hemisphere, where more than 250 intense extratropical cyclones develop every year on average. The number of yearly storms in southern Hemisphere areas is also high (around 200). For swell propagation over long distances, however, the number of storms per year is as relevant as the presence of continental mass barriers that may block the great circle propagation of swell energy.

Northern Atlantic and Pacific Ocean basins are separated by land masses that also limit their connection to other oceanic regions. On the other hand, a circumpolar oceanic zone free of land barriers connects all ocean basins in the Southern Hemisphere, creating great-circle "lanes" open to the propagation of southern swell toward virtually all global ocean basins. These differences are illustrated in Fig. 4, showing the global distribution of annual mean H_s contributed by ETSI and ETNA.

The broad connection between southern ocean basins allows ETSI swells to freely penetrate adjacent ocean basins, as illustrated in Fig. 4(a). The "wake-like" average H_s patterns indicate that ETSI swells spread energy toward both Northern and Southern Hemispheres. Conversely, Fig. 4(b) shows that the presence of swell propagating from ETNA is mostly limited to the Atlantic Ocean basin.

The combination of storm numbers/durations and the geographic characteristics of different ocean basins, therefore, determines the more general properties of how swells generated in most Northern and Southern Hemisphere generation areas propagate throughout the global ocean. Area-specific differences arise due to other characteristics of each selected generation zone, which will be explored in the following sections.

6.1.1. Southern Hemisphere extratropical areas

Storms within ETSA, ETSP and ETSI typically propagate to the east, below 40°S. Maximum storm densities occur on the western sides of these ocean basins near 50°S. Reflecting the major storm advection patterns, a large number of ETSA and ETSI swells freely propagate eastward into the tropical and subtropical latitudes of the Indian and Pacific Oceans, respectively, as shown in Figs. 4(a) and 5(a). Although somewhat constrained due to the relatively small Drake passage between the south Pacific and Atlantic Oceans, these patterns are also a dominant feature of ETSP swells (Fig. 5(b)).

Eastward propagating ETSA swell energy spreads through the entire Indian Ocean, reaching the coasts of Thailand, Indonesia and southwestern Australia, and penetrating as far as the Tasman Sea. Fig. 7(a) indicates that ETSA swell is a significant component of the Indian ocean wave climate during most of the year. Similarly, ETSI swells spread throughout a large area of the
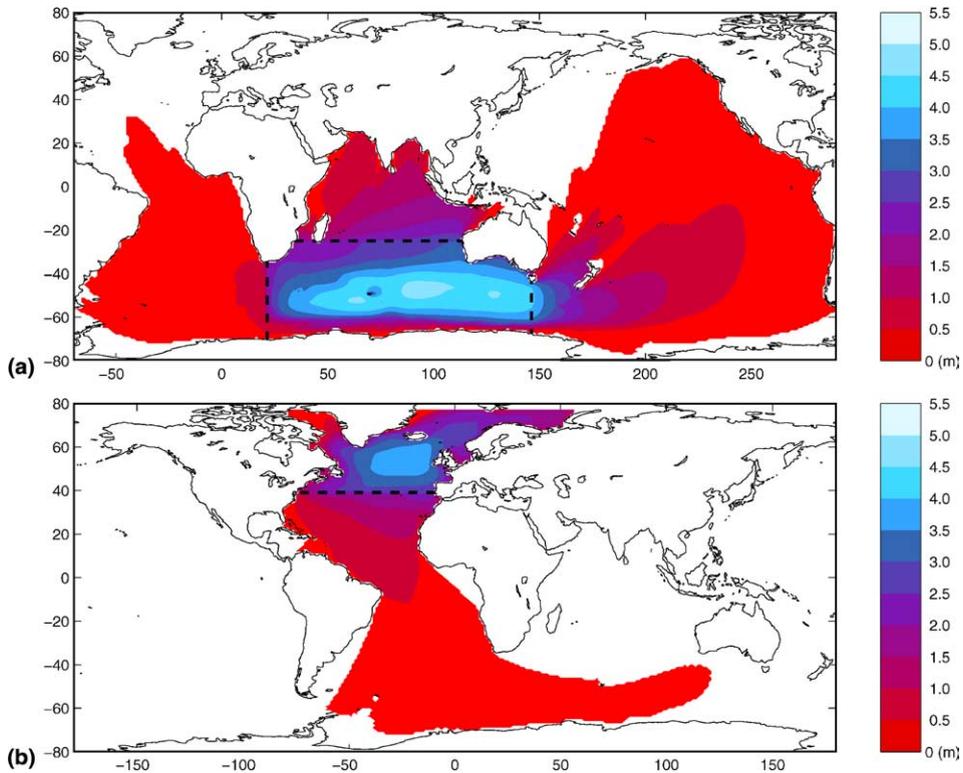
Fig. 4. Global fields of annual mean H_s (year 2000) originating from: (a) ETSI and (b) ETNA. A cutoff level is imposed at locations with persistence $\leqslant$ 1 day.

Pacific ocean. This suggests a significant impact on the wave climatology in the southern Pacific (see Fig. 4(a) and Fig. 7(c)). The eastward penetration of ETSP swell into the Atlantic Ocean is also a persistent component of the wave climate in the southernmost parts of the Atlantic Ocean basin (Fig. 5(b)).

The northward propagation of southern ocean extratropical swells is an important feature of the wave climate in the northern oceanic basins. ETSP swells have propagation patterns with several interesting features, as seen in the distribution of yearly maximum H_s in Fig. 6(b). Maximum H_s pathways suggest a complex network of dynamic storm fetches, which generate swell systems reaching the Canadian coast, the Tuamotu Islands, the Aleutian archipelago and the coasts of Japan and Russia.

Near the South American coast, ETSA storms moving toward the northwest generate swells reaching the western coast of Africa and the entire North Atlantic basin (Fig. 5), mostly during autumn and winter. ETSI swell is a persistent feature of the wave climate year round in the northern Indian Ocean basin (Figs. 4 and 6). The dominant feature associated with this pattern is the propagation of intense swell systems toward the southwestern coast of Indonesia and Australia, which also reach the coasts of Burma and India.

Another interesting Southern Hemisphere extratropical swell pattern is a persistent westward transport of wave energy, against the dominant storm advection direction. These patterns have
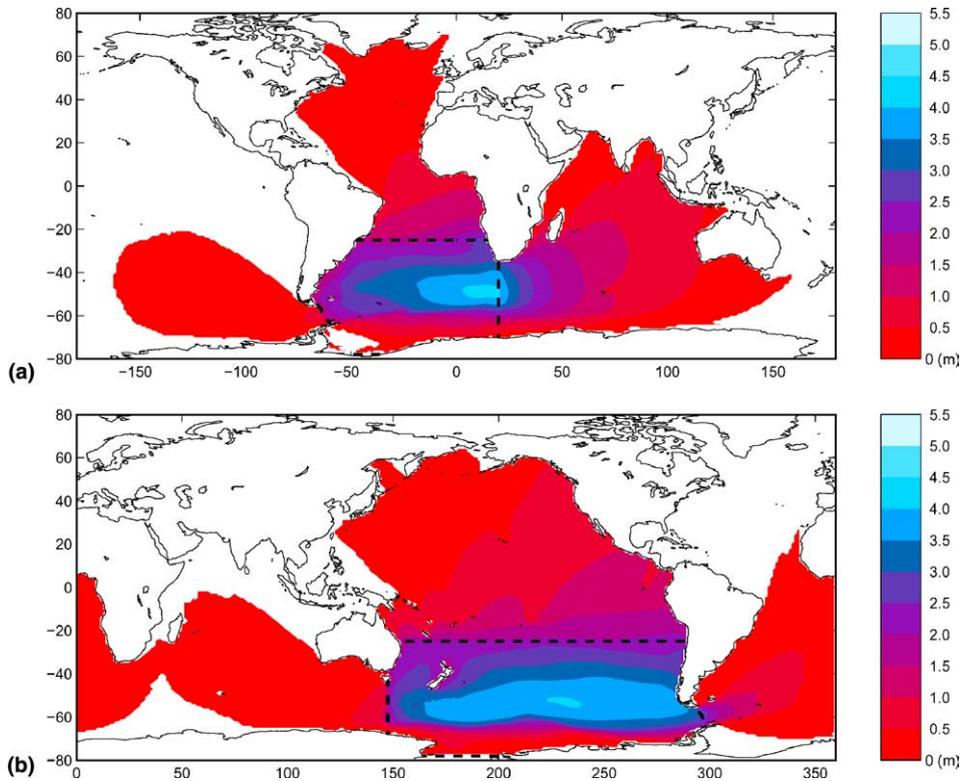
Fig. 5. Global fields of annual mean H_s originating from: (a) ETSA and (b) ETSP.

not been described so far in the scientific literature, probably due to the lack of systematic measurements in these areas. Figs. 6 and 7 provide a spectacular view of these westward swell signals. A seasonal analysis indicates that westward swells are observed year round, with similar intensity and persistence. This results from a balance between the ice coverage near Antarctica and the location/intensity of storms. In summer, storms are weaker but westward swells are generated in a broader area near the connection between ocean basins. In winter, storms are more intense but develop over reduced oceanic areas north of Antarctica.

The most striking westward swell patterns seen in Figs. 4–7 originate from ETSI. They occur over more than half the year, spreading over the entire south Atlantic basin and occasionally into the North Atlantic. Westward ETSP swells also spread over a significant part of the southern Indian Ocean, as shown in panel (b) of Figs. 5–7, and contribute more significantly to the wave climate near the south and southwestern coasts of Australia. ETSA swells also have a noticeable westward penetration into the south Pacific through the Drake Passage (Figs. 5(a), 7(a) and 6(a)).

6.1.2. Northern Hemisphere extratropical areas

ETNA and ETNP are separated from each other by land masses and the Arctic ice cap. Despite significant differences in basin geometry, the yearly statistics and properties of storms in both areas are very similar, as shown in Table 1. A comparison between Fig. 4(b) and Fig. 8(a),
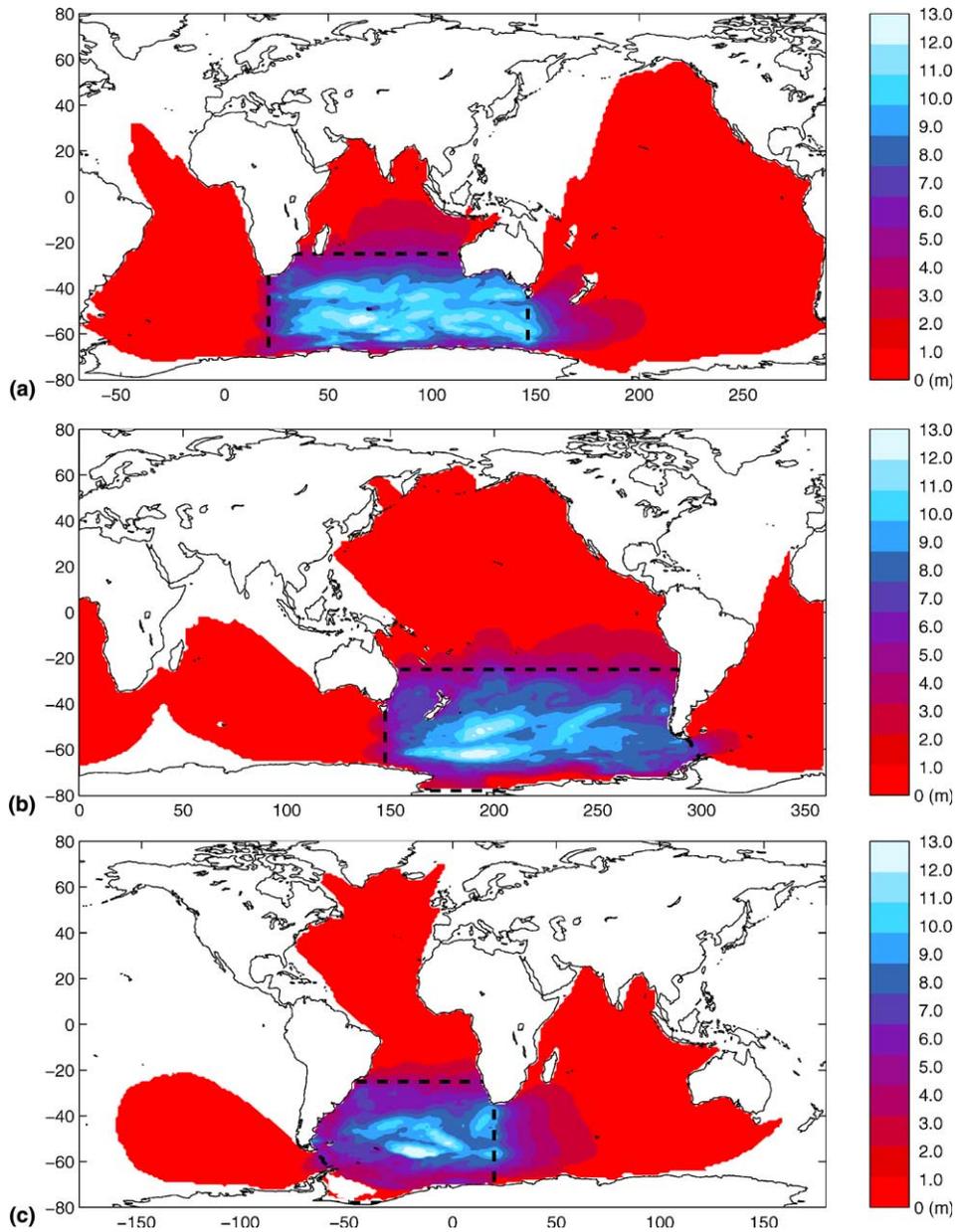
Fig. 6. Global fields of annual maximum H_s originating from: (a) ETSA, (b) ETSP and (c) ETSI.

however, indicates that swell systems originating from ETNP have a much larger impact to the global wave climate than ETNA swells.

While ETNA is constrained by surrounding continental land masses, ETNP is located above a free connection between north and south Pacific basins. In addition, ETNP's meridional extent is twice as long as ETNA's, favoring the development of cumulative fetches in the dominant,
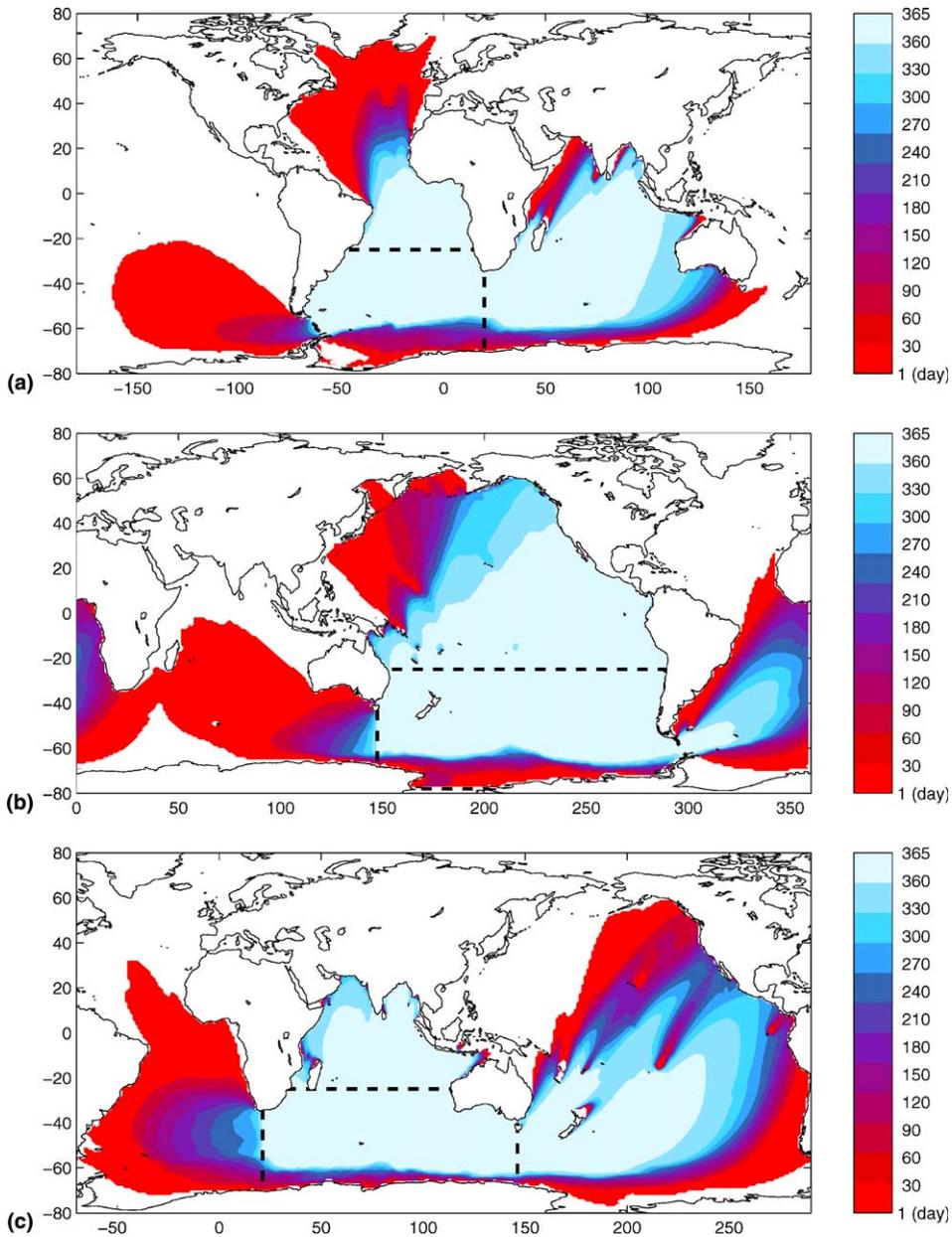
Fig. 7. Global fields of persistence of waves originating from: (a) ETSA, (b) ETSP and (c) ETSI.

eastward storm propagation direction. The geo-oceanographic characteristics of ETNP, therefore, result in the generation of swell systems that propagate freely into most of the south Pacific basin.

Fig. 8(b) shows that persistence parameter values of ETNP swells in the south Pacific are high (6 months to a full year), with annual mean H_s ranging from 0.5 to 2.0 m. Maximum ETNP swell H_s can be as high as 1.5–2.0 m near Polynesia and the coasts of Chile, for example. Swells
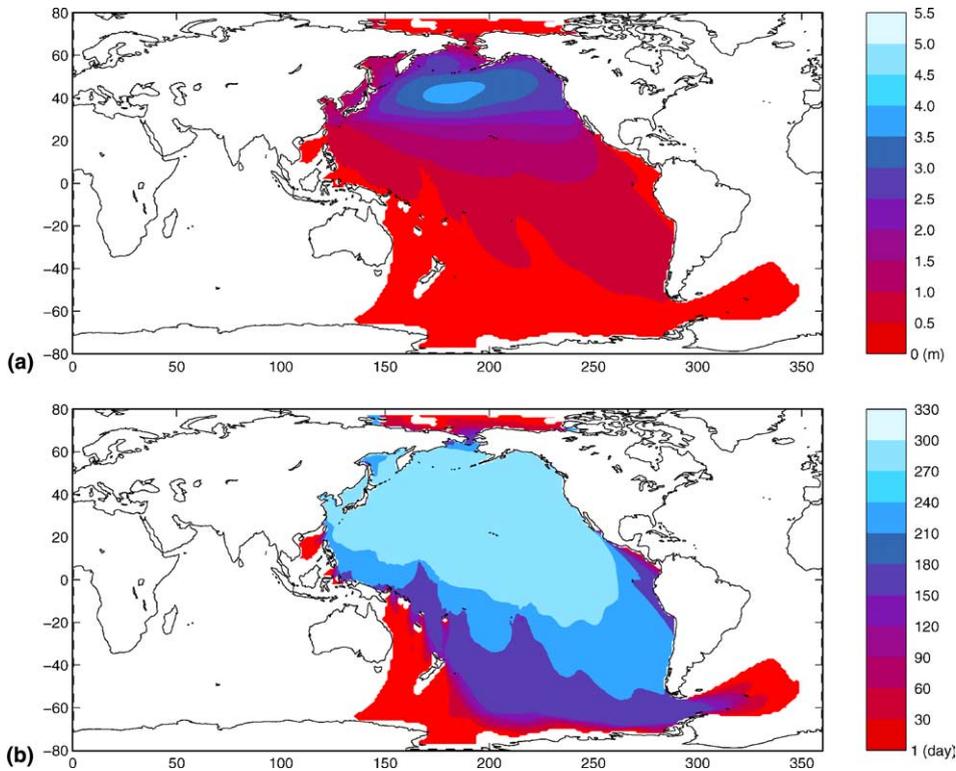
Fig. 8. Global fields of: (a) annual mean H_s and (b) persistence for waves originating from ETNP.

generated in the western sector of ETNP occasionally make their way through the Drake passage, between South America and Antarctica, reaching the southern limits of the South Atlantic basin. This striking feature persists during most of the year (180 days near the Drake passage), breaking down during Northern Hemisphere summer.

Continental land masses significantly restrict the propagation of ETNA swell, as seen in Fig. 4(b). For that reason, during Northern Hemisphere summer, ETNA swells are mostly confined to the northern latitudes. In winter, "explosive" storms develop near the strong surface temperature gradients that develop near the Gulf stream (Sanders and Gyakum, 1980). Consequently, ETNA winter swells spread throughout the south Atlantic, reaching the northeast coast of Brazil and some areas in western Africa (Fig. 4(b)). Winter ETNA swells also penetrate into the southern Indian ocean following great circle "gateways", generating an impressive pattern that reaches the proximity of southwestern Australia (Fig. 9).

6.2. Tropical storm areas

Tropical storm events are generally longer and often more intense than the average extratropical storm, as suggested by data in Table 1. Therefore, despite the relatively smaller absolute number of events, tropical areas generate swells that also contribute significantly to the global wave climate. Most tropical areas generate swells that are important for the wave climate in other
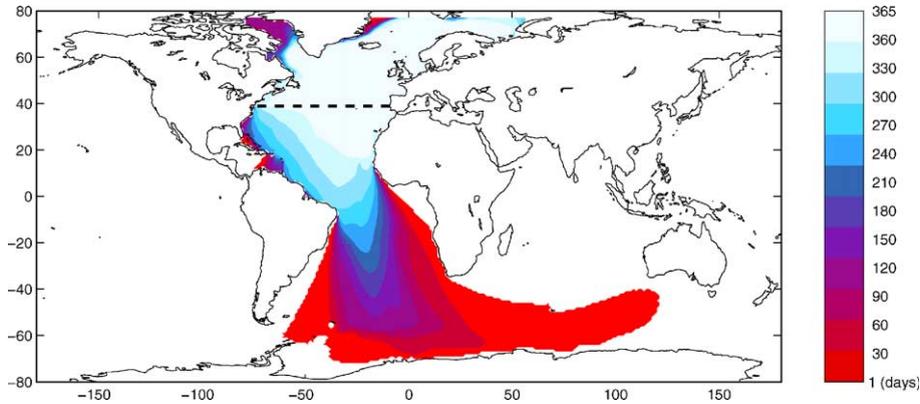
Fig. 9. Global fields of persistence of waves originating from ETNA.

regions. The exceptions are TESP and TSAO, where tropical storms rarely evolve over the ocean. Swells generated in these two areas result from the occasional penetration of extratropical storms from higher latitudes, which are generally in their final life cycle stages.

TNIO storms are constrained by the presence of land masses. Consequently, they have limited impact on the global wave climate. Although local wave systems can be very rough (see Young and Holland, 1996; and Alves and Young, 2004), Fig. 10 shows that TNIO swells rarely venture further than the mid-latitudes in the South Indian Ocean (Northern Hemisphere winter), or the southeastern Indian Ocean near the Australian coast (Northern Hemisphere summer).

TWNP swells propagate predominantly toward the northern Pacific basin, with little penetration toward other regions (Fig. 11), as a consequence of a very consistent northwestward storm propagation pattern. However, TWNP swells occasionally "percolate" through the Polynesian Islands northeast of Australia to penetrate the Coral sea, as seen in Fig. 11.

The remaining tropical areas have a more significant number of tropical storms per year (see Table 1) and consequently, a higher relevance to the global wind-wave climate. During Southern Hemisphere summer, spring and autumn TWSP swells are predominantly generated by tropical
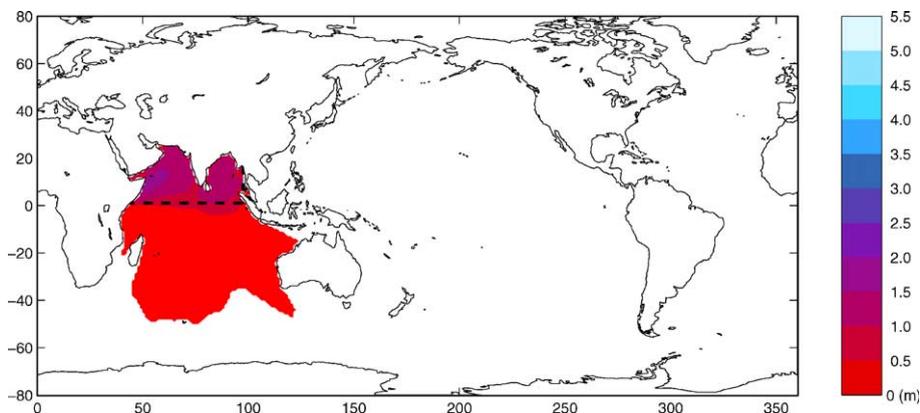
Fig. 10. Global fields of annual mean H_s originating from TNIO.
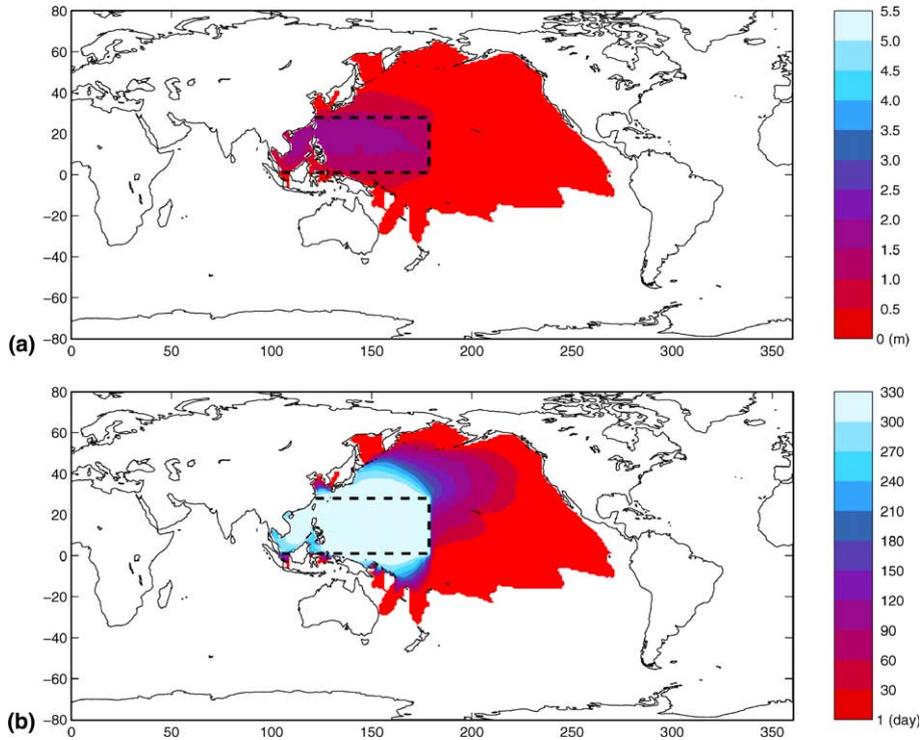
Fig. 11. Global fields of: (a) annual mean H_s and (b) persistence for waves originating from TWNP.

storms moving south- and southeastward. TWSP swells cross the Tasman Sea, penetrating the South Atlantic Ocean, eventually reaching the Drake passage (Fig. 12(a)). During southern Hemisphere winter, extratropical storms occasionally propagate across the southern limits of TWSP, generating swells that reach high latitudes in the northern Pacific basin (Fig. 12(b)).

During the summer, tropical storms in the TNAO move mostly westward, generating swell systems that propagate to high latitudes in the North Atlantic and the Gulf of Mexico, with little impact on other regions (Fig. 13(a)). During winter, eastward propagating extratropical storms observed in the TNAO generate swells that propagate to the southeast throughout the South Atlantic, eventually reaching the southern Indian Ocean. Due to a reduced concentration of Antarctic ice in that season, this pattern occasionally extends as far as the southwestern coast of Australia (Fig. 13(b)).

Storm tracks in Fig. 1 and data in Table 1 indicate that the TSIO and TENP are predominantly populated by tropical storms and relatively less exposed to extratropical storms than other tropical areas. TSIO and TENP swells have a significant impact on the wave climate in adjacent oceanic regions, thus showing the importance of tropical storms in generating swells capable of propagating long distances.

Tropical storms in the TENP occur predominantly between May and November. TENP storms have a strong westward propagation component, leading to the development of cumulative or dynamic westward fetches. Consequently, TENP swells propagate freely into the western and high
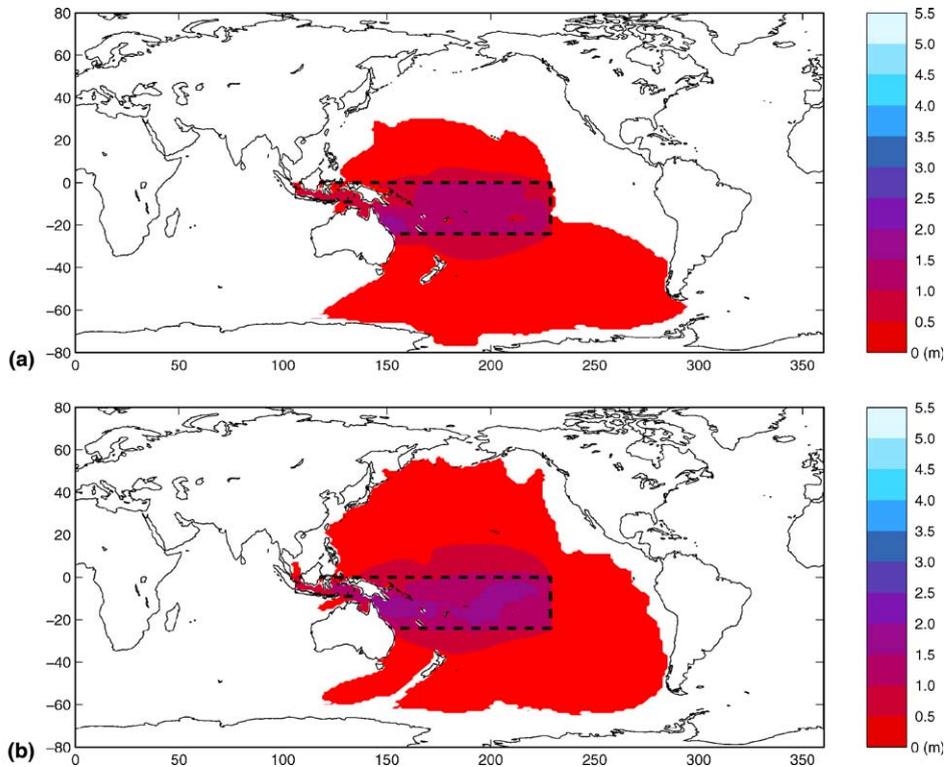
Fig. 12. Global fields of seasonal mean H_s originating from TWSP Southern Hemisphere: (a) summer and (b) winter.

latitude regions of the North Pacific (year round), the south Pacific basin (about 6 months in the year) and, occasionally, into the Tasman Sea (about 30–60 days in the year), eventually approaching the Antarctic region (Fig. 14).

TSIO generates swell systems that spread freely onto large areas of the Southern Indian Ocean. A spectacular feature of TSIO swells is their westward penetration into the South Atlantic Ocean. Fig. 15(a) shows that this pattern is observed consistently, with persistence between 30 and 180 days in the central South Atlantic, where maximum H_s ranged from 0.5 m to 1.0 m (Fig. 15(b)). TSIO swells also produce a significant signal in the higher latitudes of the south Indian basin, reaching as far as the westernmost limits of the Tasman Sea.

7. Summary and concluding remarks

A numerical modeling technique for studying the contribution of ocean swell to the global wind-wave climate is proposed. This technique allows for a qualitative evaluation of the contribution of swells from different ocean basins to the global wind-wave climate. In this technique, windseas are generated in discrete oceanic areas by numerical modeling. Discrete generation areas are isolated from adjacent regions of the global ocean, where surface winds are switched off but swells are allowed to propagate freely.
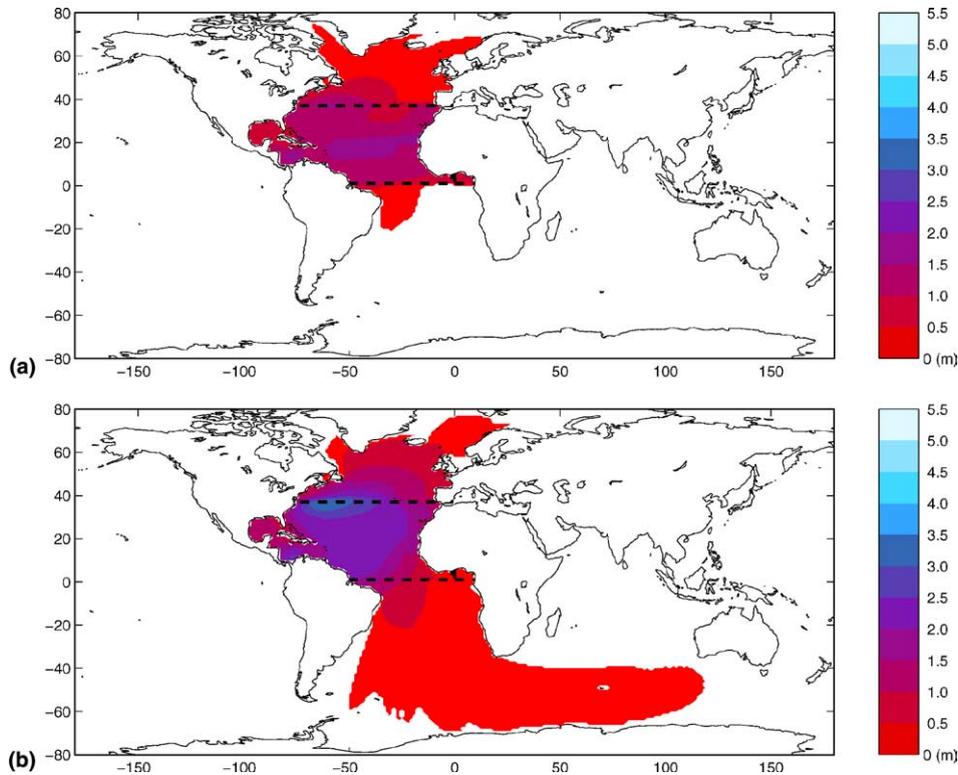
Fig. 13. Global fields of seasonal mean H_s originating from TNAO Northern Hemisphere: (a) summer and (b) winter.

Reflecting a compromise between reducing the computational costs and maximizing the consistency of discrete areas, in terms of storm history and climatology, a total of 13 generation areas are selected within tropical and extratropical zones of the global ocean. Simulations of windsea generation within selected areas and their propagation as swell throughout the global ocean are made using the state-of-the-art wind-wave model WAVEWATCH III, over a period of two model years.

A preliminary climatological analysis of the major patterns associated with swells generated within selected areas is presented, along with a brief analysis of their importance to the wave climate in remote oceanic basins. Several features of relevance for a global swell climatology are confirmed or identified, some of the latter not previously reported or explored in the known scientific literature, as follows:

- The global distribution of continental land masses is a major factor determining the impact of swells on the global wind-wave climate.
- Swells generated in extratropical areas of the southern oceans spread energy throughout the entire global ocean, and are a potentially important component of the wave climate in most ocean basins in both hemispheres.
- Contradicting the common wisdom, extratropical areas in the Southern Hemisphere generate robust swell systems that propagate westward against the predominant storm advection direction.
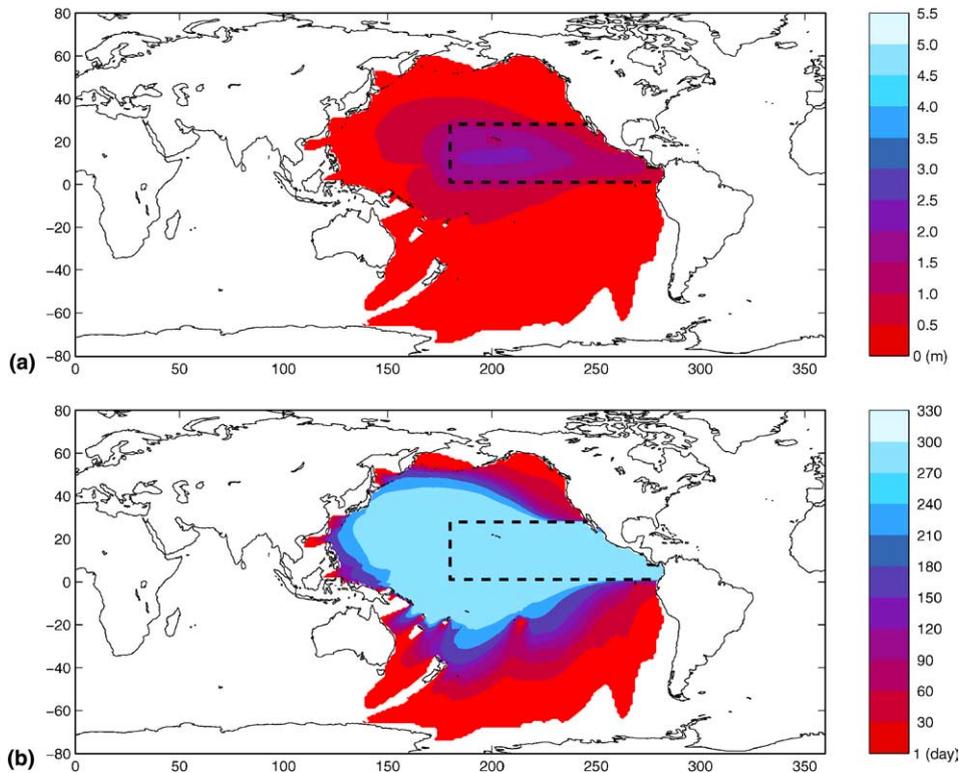
Fig. 14. Global fields of: (a) annual mean H_s and (b) persistence for waves originating from TENP.

- Despite the presence of massive land mass barriers, extratropical swells from the Northern Hemisphere contribute significantly to the wave climate in remote locations.
- Swells generated in most tropical areas exposed to tropical storms contribute significantly to the global wave climate.
- Subgrid shadowing in a global scale model indicate that oceanic islands significantly constrain the propagation of swells.

The validity of the technique devised above is verified through a comparison of the sum total of energies from segmented wave fields against the total energy fields from a reference model run made with the full, unsegmented global wind fields. The results of this verification lead to the following conclusions:

- Mean annual biases and RMS errors of the reconstructed wave fields are generally within reasonable limits for the purpose of global climatology studies in most oceanic regions.
- Near the generation area boundaries, higher relative errors in reconstructed fields result from the artificial interruption of dynamic wind fetches associated with moving storms or zonal winds.
- Regions of higher relative error statistics occur mostly in small regions near area boundaries, not penetrating significantly into the majority of regions covered by the global ocean.
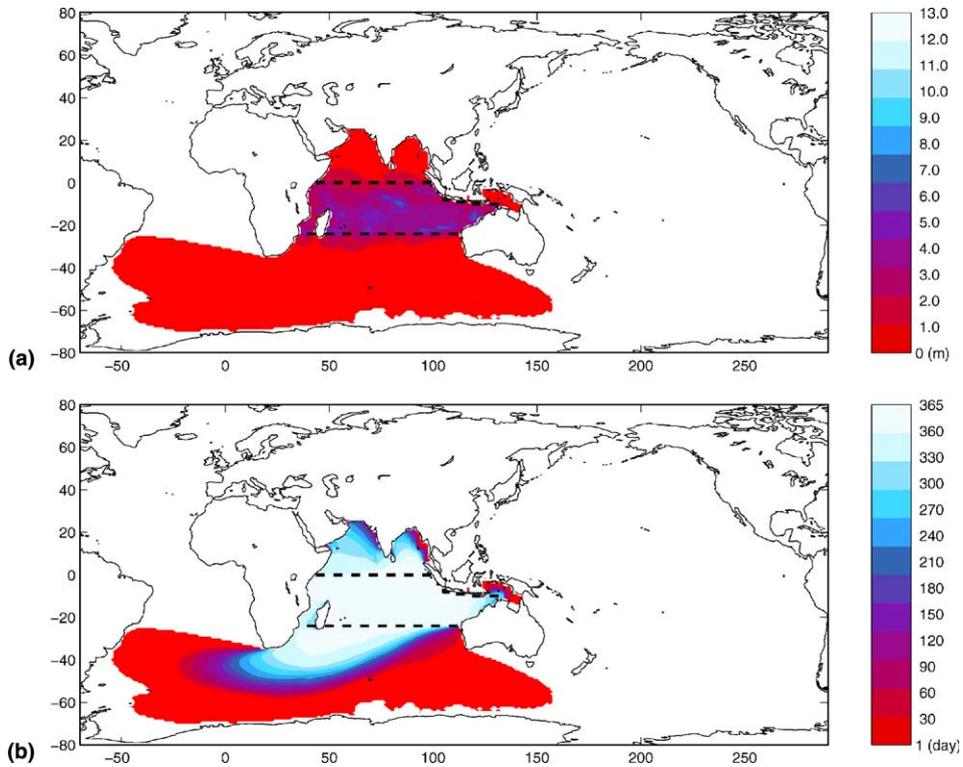
Fig. 15. Global fields of: (a) persistence and (b) maximum H_s for waves originating from TSIO.

- Relative errors of reconstructed wave fields may be assumed to be of secondary importance in a global swell climatology.
- Localized areas with higher relative errors indicate potential limitations in the wind segmentation technique for local wave climate studies, that warrants further investigation.
- Results indicate potential sources of errors for wave prediction systems in which smaller grids are not nested into larger-scale models covering potential sources of swell.

Results presented in this manuscript indicate that a wind-wave modeling technique based on the segmentation of wind fields provides a valid framework for the purpose of studying climatological aspects of swell fields on a global scale.

Advanced Computing (APAC), the South Australian Partnership for Advanced Computing (SAPAC) and NCEP/NOAA.

References

Alves, J.H.G.M., Young, I.R., 2004. On estimating extreme wave heights using combined Geosat, Topex/Poseidon and ERS-1 altimeter data. Appl. Ocean Res. 25 (4), 167–186.

Ardhuin, F., O'Reilly, W.C., Herbers, T.H.C., Jessen, P.F., 2003a. Swell transformation across the continental shelf. Part I: Attenuation and directional broadening. J. Phys. Oceanogr. 33 (9), 1921–1939.

Ardhuin, F., O'Reilly, W.C., Herbers, T.H.C., Jessen, P.F., 2003b. Swell transformation across the continental shelf. Part II: Validation of a spectral balance equation. J. Phys. Oceanogr. 33 (9), 1940–1953.

Barber, N.F., Ursell, F., 1948. The generation and propagation of ocean waves and swell. I. Wave periods and velocities. Philos. Trans. Roy. Soc. London 240A, 527–560.

Chen, G., Belcher, S.E., 2000. Effects of long waves on wind-generated waves. J. Phys. Oceanogr. 30 (9), 2246–2256.

Chen, G., Chapron, B., Ezraty, R., Vandemark, D., 2002. A global view of swell and wind sea climate in the ocean by satellite altimeter and scatterometer. J. Atmos. Ocean. Technol. 19 (11), 1849–1859.

Donelan, M.A., 1987. The effect of swell on the growth of wind waves. Johns Hopkins APL Tech. Digest 8, 18–23.

Donelan, M.A., Drennan, W.M., Katsaros, K.B., 1997. The air–sea momentum flux in conditions of wind sea and swell. J. Phys. Oceanogr. 27 (10), 2087–2099.

Drennan, W.M., Kahma, K.K., Donelan, M.A., 1999. On momentum flux and velocity spectra over waves. Bound. Layer Meteorol. 92, 489–515.

Gerling, T.W., 1992. Partitioning sequences and arrays of directional wave spectra into component wave systems. J. Atmos. Ocean. Technol. 9, 444–458.

Gill, A.E., 1982. Atmosphere–Ocean Dynamics. Academic Press, NY, p. 662.

Grachev, A.A., Fairall, C.W., 2001. Upward momentum transfer in the marine boundary layer. J. Phys. Oceanogr. 31, 1698–1711.

Grachev, A.A., Fairall, C.W., Hare, J.E., Edson, J.B., 2003. Wind stress vector over ocean waves. J. Phys. Oceanogr. 33, 2408–2429.

Grumbine, R.W., 1996. Automated passive microwave sea ice concentration analysis at NCEP. NWS/NCEP/OMB Technical Note 120, 13p.

Gulev, S.K., Hasse, L., 1998. North Atlantic wind waves and wind stress fields from voluntary observing ship data. J. Phys. Oceanogr. 28 (6), 1107–1130.

Gulev, S.K., Zolina, O., Grigoriev, S., 2001. Extratropical cyclone variability in the Northern Hemisphere winter from the NCEP/NCAR reanalysis data. Climate Dyn. 17, 795–809.

Hanson, J.L., Phillips, O.M., 2001. Automated analysis of ocean surface directional wave spectra. J. Atmos. Ocean. Technol., 277–293.

Holthuijsen, Tolman, 1997. Effects of the Gulf stream on ocean waves. J. Geophys. Res. 96 (C7), 12,755–12,771.

Keable, M., Simmonds, I., Keay, K., 2002. Distribution and temporal variability of 500 hPa cyclone characteristics in the Southern Hemisphere. Int. J. Climatol. 22, 131–150.

Kinsman, B., 1965. Wind Waves. Prentice-Hall, Englewood Cliffs, NJ, p. 676.

Klinck, J.M., Nowlin Jr., W.D., 2001. Antarctic Circumpolar Current, in Encyclopedia of Ocean Science, first ed. Academic Press, New York, 151–59.

Lambert, S.J., Sheng, J., Boyle, J., 2002. Winter cyclone frequencies in thirteen models participating in the Atmospheric Model Intercomparison Project (AMIP1). Climate Dyn. 19, 1–16.

Moorthi, S., Pan, H.-L., Caplan, P., 2001. Changes to the 2001 NCEP operational MRF/AVN global analysis/forecast system. Technical Procedures Bulletin No. 484, National weather Service, NOAA, US Department of Commerce. Available from: <http://www.nws.noaa.gov/om/tpb/>.

Munk, W.H., 1947. Tracking storms by forerunners of swell. J. Meterol. 4 (2), 45–57.

Munk, W.H., Miller, G.R., Snodgrass, F.E., Barber, N.F., 1963. Directional recording of swell from distant storms. Philos. Trans. R. Soc. London A255, 505–584.

Paciorek, C.J., Risbey, J.S., Ventura, V., Rosen, R.D., 2002. Multiple indices of Northen Hemisphere cyclone activity, winters 1949–99. J. Climate 15, 1573–1590.

Sanders, F., Gyakum, J.R., 1980. Synoptic–dynamic climatology of the ''bomb''. Mon. Weather Rev. 108, 1589–1606.

Shyu, J.H., Phillips, O.M., 1990. The blockage of gravity and capillary waves by longer waves and currents. J. Fluid Mech. 217, 115–141.

Simmonds, I., Keay, K., 2000. Mean Southern Hemisphere extratropical cyclone behavior in the 40-year NCEP-NCAR reanalysis. J. Climate 13, 873–885.

Sinclair, M.R., 2002. Extratropical transition of southwest Pacific tropical cyclones. Part (I) climatology and mean structure changes. Mon. Weather Rev. 130, 590–609.

Smedman, A.S., Larsen, X.G., Hogstrom, U., Kahma, K.K., Pettersson, H., 2003. Effect of sea state on the momentum exchange over the sea during neutral conditions. J. Geophys. Res. 108 (C11), 3367.

Snodgrass, F.E., Groves, G.W., Hasselmann, K.F., Miller, G.R., Munk, W.H., Powers, W.M., 1966. Propagation of swell across the Pacific. Philos. Trans. R. Soc. London A259, 431–497.

Teixeira, M.A.C., Belcher, S.E., 2002. On the distortion of turbulence by a progressive surface wave. J. Fluid Mech. 458, 229–267.

Tolman, H.L., 1998a. Validation of NCEP's ocean winds for the use in wind wave models. Global Atmos. Ocean Sys. 6, 243–268.

Tolman, H.L., 1998b. Validation of a new global wave forecast system at NCEP. In: Edge, B.L., Helmsley, J.M. (Eds.), Ocean Wave Measurements and Analysis. ASCE, pp. 777–786.

Tolman, H.L. (2002a) User manual and system documentation of WAVEWATCH-III version 2.22. NOAA/NWS/NCEP/OMB Technical Note 222, 133p.

Tolman, H.L. (2002b) Validation of WAVEWATCH III version 1.15 for a global domain. NOAA/NWS/NCEP/OMB Technical Note No. 213, 33p (2.7 Mb pdf file, in color).

Tolman, H.L., 2003. Treatment of unresolved islands and ice in wind wave models. Ocean Model. 5, 219–231.

Tolman, H.L., Balasubramaniyan, B., Burroughs, L.D., Chalikov, D.V., Chao, Y.Y., Chen, H.S., Gerald, V.M., 2002. Development and implementation of wind generated ocean surface wave models at NCEP. Weath. Forecast. 17, 311–333.

Wingeart, K.M., O'Reilly, W.C., Herbers, T.H.C., Wittmann, P.A., Jenssen, R.E., Tolman, H.L., 2001. Validation of operational global wave prediction models with spectral buoy data. In: B.L., Edge, J.M., Hemsley (Eds.), Ocean Wave Measurement and Analysis, San Francisco, CA. ASCE, pp. 590–599.

Young, I.R., Holland, G., 1996. Atlas of the Oceans: Wind and Wave Climate. Pergamon Press, Berlin, p. 241.